



Research on micro-cutting mechanism of CoCrFeNiAl_x high-entropy alloy fiber–reinforced aluminum matrix composites

Ping Zhang^{1,2} · Shunxiang Wang¹ · Xiujie Yue^{2,3} · Zhenyong Lin¹ · Yeran Gao¹ · Songting Zhang¹

Received: 23 July 2023 / Accepted: 2 December 2023 / Published online: 13 December 2023
© The Author(s), under exclusive licence to Springer-Verlag London Ltd., part of Springer Nature 2023

Abstract

This study aims to investigate the micro-cutting mechanism of CoCrFeNiAl_x short fiber–reinforced 7A09 aluminum matrix composites. By setting different material constitutive models, material failure, and evolution criteria for each reinforcing phase, orthogonal cutting simulations were conducted at four typical angles (0°, 45°, 90°, 135°). The effects of fiber angle, volume fraction, and Al element content on cutting forces, cutting temperatures, chip morphology, and residual stresses were investigated under different cutting parameters. Micro-cutting experiments were also conducted to verify the micro-cutting of CoCrFeNiAl₀ fiber–reinforced aluminum matrix composites. The results show that the cutting depth is positively correlated with cutting forces, and the increase in cutting force is approximately 51% when the cutting depth increases from 30 to 60 μm. Both cutting forces increase and then decrease with increasing cutting speed and fiber angle. The cutting forces decrease first and then increase with the increasing Al element content in the fibers. Cutting forces are positively correlated with the volume fraction of fibers in the workpiece, and compared to the workpiece without fibers, the cutting force increases by approximately 22% at a fiber content of 15 vol%. The cutting temperature gradually increases with increasing cutting depth and cutting speed. The cutting temperature first increases and then decreases with increasing fiber angle, and when the fiber angle increases from 45 to 135°, the cutting temperature decreases by 44%. The cutting temperature first decreases and then increases with the increasing Al element content in the fibers. The integrity of the cutting surface is positively correlated with cutting depth, Al content in the fibers, and fiber volume fraction. Multiple and irregular chip fractures are observed when the fiber angle is 45° or 90°, while the integrity of the chips improves when the fiber angle is 0° or 135°. The chip layer exhibits block-like fracture when the fiber volume fraction reaches 15 vol%. The peak residual compressive stress is negatively correlated with cutting depth, cutting speed, and Al content in the fibers, and the peak position moves away from the machined surface with the increase of the first two factors. The peak residual compressive stress is positively correlated with fiber angle and fiber content in the workpiece, and when the fiber angle is 135° or the volume fraction is 15 vol%, the peak position is significantly away from the machined surface.

Keywords Fiber-reinforced composites · Cutting forces · Cutting temperatures · Chip morphology · Residual stresses

1 Introduction

Aluminum matrix composites (AMCs) have been widely used in aerospace, automotive manufacturing, electronics devices, and other fields due to their high strength-to-weight ratio, excellent corrosion resistance, and good thermal conductivity [1,2]. High-entropy alloys (HEAs) are a new type of material with a randomly arranged atomic structure that provides outstanding mechanical properties and can form a good metallurgical interface with aluminum. The addition of short fibers made of HEAs to AMCs can further enhance the strength, ductility, and fracture toughness of the material. However, the processing of composite materials is

✉ Ping Zhang
zpqdhxy@126.com

¹ College of Mechanical and Power Engineering, Guangdong Ocean University, Zhanjiang, China

² College of Intelligent Manufacturing, Qingdao Huanghai University, Qingdao 266520, China

³ College of Intelligent Manufacturing, Qingdao University of Technology, Qingdao 266520, China

challenging due to the significant differences in mechanical properties between the fibers and the matrix. Therefore, the processing of fiber-reinforced polymers (FRPs) typically involves various types of damage, such as fiber pull-out or fracture, matrix cracking, and fiber-matrix delamination [3,4].

Experimental research on FRP processing has made significant progress to date. Wang et al. conducted experimental studies on the orthogonal cutting mechanism of single-crystal diamond tools cutting unidirectional graphite/epoxy composites [5]. The results showed that the chip formation mechanism is closely related to the fiber volume fraction and orientation. Wang et al. [6] investigated the machining performance of unidirectional fiber-reinforced composites under orthogonal cutting conditions and found that fiber orientation has a significant influence on the subsurface damage and its mechanism in machined components. Three distinct deformation zones, namely, the fragmentation zone, the compression zone, and the rebound zone, were observed when the fiber orientation was 90° . In addition to the fiber volume fraction and orientation, the processing performance of FRPs is also influenced by the material and geometry of the cutting tools. Marques et al. [7] drilled carbon fiber/epoxy laminates using four different geometric shapes of drills and achieved the goal of the study by using different cutting parameters and the four drill geometries. The results showed that the drilling effect of the drill with a reduced chisel edge indentation was the best, reducing surface damage by 2%. Shyha et al. [8] drilled carbon fiber-reinforced plastic laminates using drills with different coatings and found that the drilling thrust produced by TiN-coated drills with conventional geometry was generally below 100 N and effectively reduced tool wear, thereby improving the machining quality. Additionally, researchers have also explored the influence of processing parameters on FRP processing. Rajasekaran et al. [9] evaluated the surface quality of carbon fiber-reinforced composite turning using fuzzy logic methods and found that the feed rate, cutting speed, and depth of cut significantly affected the surface roughness of the composite material. Palanikumar et al. [10] concluded that high cutting speeds, large depths of cut, and low feed rates ensure good surface quality. However, these studies are mainly limited to traditional processing methods such as turning, milling, drilling, and grinding, and still face challenges in achieving satisfactory surface integrity. To reveal the processing mechanisms, numerical simulation techniques, particularly finite element-based methods, have gradually been applied to the study of FRP cutting mechanisms and process improvement. Cheng et al. [11] established a thermo-mechanical coupling model of orthogonal cutting forces for unidirectional CFRP laminates and revealed the deformation and cutting force variation patterns of carbon

fiber-reinforced composites at the microscopic scale, achieving observation results consistent with experiments. It can be seen that when modeling FRPs, it is necessary to establish multiple fiber-reinforced bodies and matrices to objectively simulate and predict the extrusion, bending, shearing, and fracture modes of the fibers and matrices under the action of cutting forces. The research progress listed above on FRP machining is mainly focused on carbon fiber-reinforced non-metallic matrices. However, since metals can form good metallurgical interfaces, and metal fibers have advantages such as good electrical conductivity, thermal conductivity, and high tensile strength, the study of metal fiber-reinforced composites is also of great significance. For example, Chen et al. [12] used a glass-encapsulated melt spinning method to prepare super-elastic Cu-Al-Ni shape memory alloy wires with diameters ranging from 10 to 500 μm , which greatly improved the brittleness of Cu-based materials and enhanced the plasticity of Cu-Al-Ni alloys. Current research on such composites mostly focuses on material preparation, with fewer articles on their processing mechanisms. Therefore, investigating the machining performance of metal fiber-reinforced composites is an important approach to promote the widespread application of such composites.

Combining the research methods of scholars on carbon fiber-reinforced composites provides rich research ideas and experience for exploring the cutting performance of high-entropy alloy fiber-reinforced aluminum composites. Therefore, in this study, a parameterized modeling method considering the fiber angle, volume fraction, and other microscopic structures was adopted. Using CoCrFeNiAl_x short fiber-reinforced aluminum-based composites as the research object, a simulation model for micro-cutting was established. By setting different material constitutive models, material failure, and evolution criteria for each phase, orthogonal cutting simulations were conducted for four typical angles (0° , 45° , 90° , 135°). The influence of different cutting parameters on the fiber angle, volume fraction, and Al element content on cutting forces, cutting temperatures, and chip morphology was studied. The research results can reflect the actual cutting process of workpieces and provide guidance for the cutting processing of aluminum-based composites.

2 Materials and methods

2.1 Geometric model establishment

The Abaqus/Explicit analysis module was selected for model construction. In this study, eight geometric models were established based on fiber angle and volume fraction [14–17], with dimensions of 0.7 mm \times 0.3 mm \times 0.2 mm

Fig. 1 Schematic diagrams of cutting models with different fiber angles

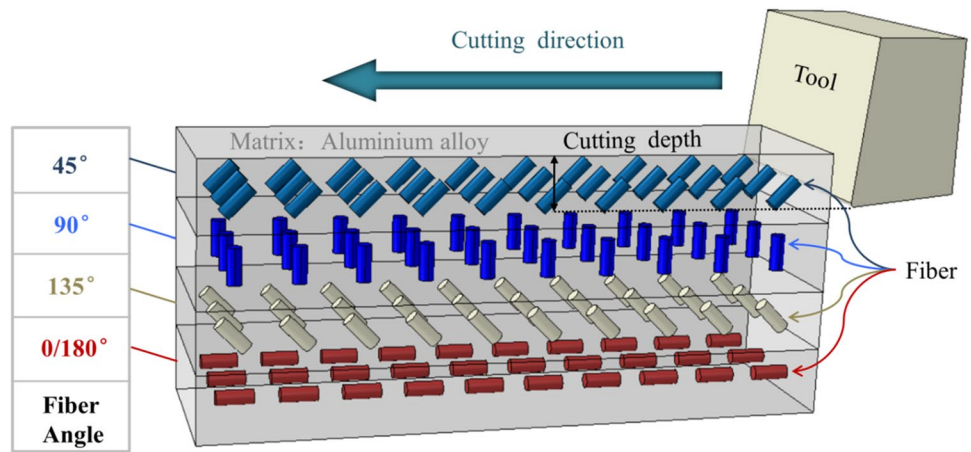


Table 1 Mechanical parameters of aluminum matrix and Al_x particles

| Material characteristics | Aluminum substrate | Al _x |
|--|-----------------------|----------------------|
| Elastic modulus/(GPa) | 68.9 | 71.7 |
| Poisson's coefficient | 0.33 | 0.33 |
| Thermal expansion/K | 2.18×10^{-5} | 1.2×10^{-8} |
| Density/(g·cm ⁻³) | 2.7 | 8.183, 7.204, 6.724 |
| Thermal conductivity/(W·m ⁻¹ ·K) | 193 | 173 |
| Specific heat/(J·kg ⁻¹ ·k ⁻¹) | 900 | 420, 499, 517 |

Table 2 J-C constitutive parameters for 7A09 aluminum alloy matrix

| A/Mpa | B/Mpa | C | n | m | T ₀ /K | T _m /K |
|--------|--------|-------|-------|-------|-------------------|-------------------|
| 518.62 | 110.25 | 0.052 | 0.524 | 0.209 | 293 | 843 |

Table 3 J-C constitutive parameters for Al_x short fibers [13]

| Al _x | A/Mpa | B/Mpa | C | n | m | T ₀ /K | T _m /K |
|-------------------|-------|-------|-------|------|------|-------------------|-------------------|
| Al ₀ | 156 | 785 | 0.06 | 0.96 | 0.86 | 298 | 1858 |
| Al _{0.6} | 594 | 971 | 0.03 | 0.71 | 0.86 | 298 | 1737 |
| Al ₁ | 1347 | 2347 | 0.015 | 0.89 | 0.86 | 298 | 1673 |

and an effective cutting length of 0.35 mm. The tool used was a hard alloy tool with the following parameters: front angle of 6°, back angle of 6°, and a blunt radius of 4 μm. The unit characteristics of the Al matrix and HEA short fibers were set as four-node coupled thermal-solid elements (C3D4T), while the unit characteristics of the tool were set as eight-node coupled thermal-solid elements (C3D8T). Fixed constraints were applied to the bottom of the model, and the contact type was set as general contact with a friction coefficient of 0.3. The fibers were uniformly distributed within the workpiece [18,19], and the tool was modeled as a rigid shell element. Schematic diagrams of the cutting models with different fiber angles are shown in Fig. 1.

Table 4 Material failure parameters

| Failure parameter | d ₁ | d ₂ | d ₃ | d ₄ | d ₅ |
|-------------------|----------------|----------------|----------------|----------------|----------------|
| alue | 0.04 | 0.75 | -1.45 | 0.04 | 0.89 |

2.2 Material models

The mechanical properties of the materials, constitutive parameters of the matrix and short fibers, and material failure parameters are shown in Tables 1, 2, 3, and 4.

2.3 Simulation plan design

In this study, CoCrFeNiAl_x short fiber–reinforced aluminum matrix composite (AMC) was selected as the workpiece model. Single-factor cutting simulations were conducted considering factors such as fiber angle [20–22], fiber volume fraction, cutting depth, cutting speed, and aluminum content in the fibers. The cutting length in this model was set as 0.35 mm. The specific simulation plan is presented in Table 5.

2.4 Experimental verification of the simulation model

To validate the accuracy of the simulation model, micro-cutting experiments were conducted on CoCrFeNiAl₀ fiber–reinforced aluminum matrix composites [23,24]. The micro-cutting process was carried out according to the Scheme 1 shown in Table 5. The micro-cutting experiments were performed on a Mitsubishi MV 820 CNC machine, and the cutting forces during the process were recorded using a YD15-111 three-component dynamometer. The experimental setup used in the experiments is shown in Fig. 2.

3 Results and discussion

3.1 Cutting force analysis

3.1.1 Influence of cutting depth on cutting force

Figure 3 shows the relationship between the main cutting force and cutting depth for a fiber angle of 45° and a volume fraction of 5vol%. From the graph, it can be observed that the cutting force is positively correlated with the cutting depth. The cutting force at 60 μm is approximately 1.5 times that at 30 μm. Furthermore, from the fluctuation curves of cutting force over time at 40 μm and 50 μm, it can be noticed that the range of cutting force fluctuations decreases with increasing cutting depth. The analysis suggests that as the cutting depth increases, the overall trend of the cutting force is to increase. This is due to the increased contact area between the tool and the workpiece, resulting in plastic deformation of the material and accumulation of cutting heat during the cutting process [25–27]. Additionally, when the fibers undergo bending and fracture, additional cutting forces

Table 5 Single-factor simulation plan

| Simulation scheme | Cutting depth/μm | Cutting speed/m·min ⁻¹ | Fiber angle/° | Fiber material | Volume fraction/vol% |
|-------------------|------------------|-----------------------------------|----------------|---|----------------------|
| 1 | 30, 40, 50, 60 | 60 | 45 | Al ₀ | 5 |
| 2 | 50 | 40, 50, 60, 70 | 45 | Al ₀ | 5 |
| 4 | 50 | 60 | 0, 45, 90, 135 | Al ₀ | 5 |
| 5 | 50 | 60 | 45 | Al ₀ , Al _{0.6} , Al ₁ | 5 |
| 6 | 50 | 60 | 45 | Al ₀ | 0, 5, 10, 15 |

Fig. 2 Experimental setup

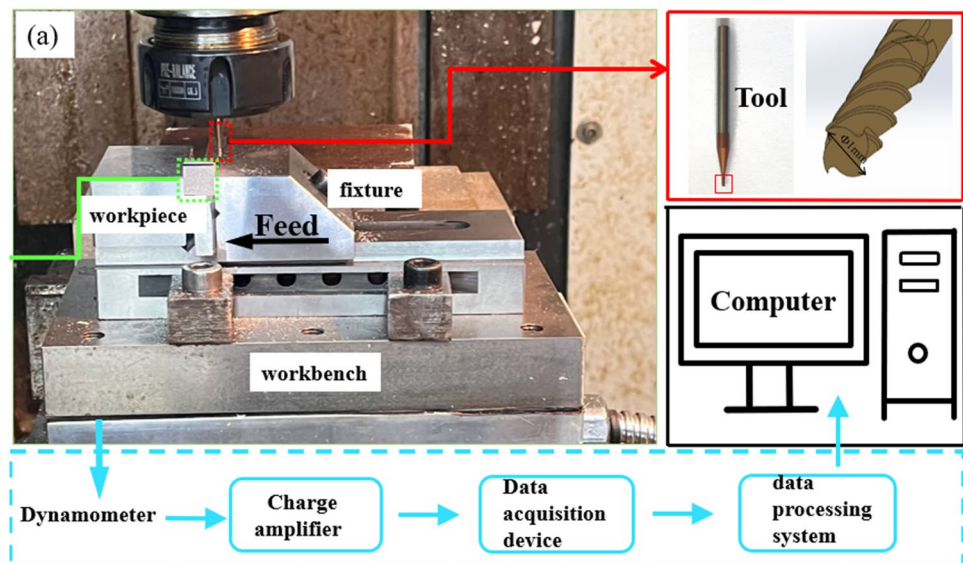
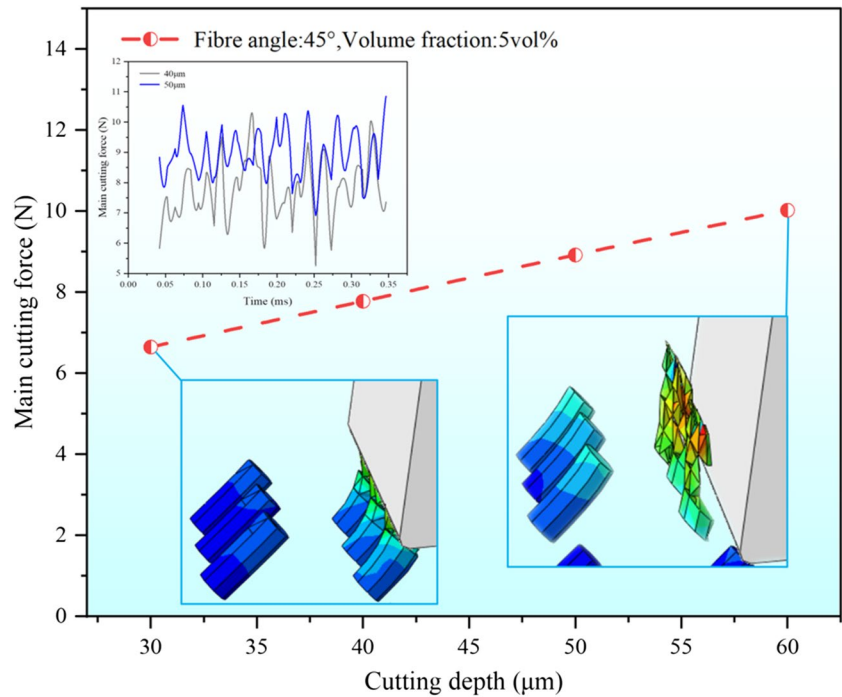


Fig. 3 Relationship between cutting depth and cutting force



are generated. From the images at 30 μm and 60 μm , it can be observed that with an increase in cutting depth, the degree of fiber bending and fracture intensifies due to the changing relative position between the tool and the fibers, ultimately leading to an overall increase in cutting force. However, in this study, the short fibers are uniformly distributed within the workpiece [28–30]. With an increase in cutting depth, the number of fibers increases, resulting in a more uniform distribution of fibers within the workpiece, thereby reducing the influence of fibers on the cutting force. Moreover, as the cutting temperature rises, the strength of the fibers decreases, reducing their impact on the cutting force and subsequently reducing the range of cutting force fluctuations. In summary, although the bending and fracture of fibers due to increasing cutting depth contribute to the overall increase in cutting force, the increase in the number of fibers and the decrease in fiber strength diminish the influence of fibers on the cutting force, resulting in a reduced range of cutting force fluctuations.

To validate the accuracy of the simulation model, the experimental values and simulated values of the main cutting force for different cutting depths were compared, and the comparison results are shown in Table 6. The comparison results indicate excellent consistency between the experimental values and simulated values of the main cutting force with varying cutting depths, and the errors between the experimental values and simulated values are all below 12%.

Figure 4 shows the surface morphology of CoCrFeNiAl_0 fiber-reinforced aluminum matrix composite under micro-cutting with different cutting depths. The surface quality showed a trend of improving first and then deteriorating, and when the cutting depth reached 60 μm , the surface showed micro-holes caused by the tearing of the reinforced phase.

3.1.2 Influence of cutting speed on cutting force

Figure 5 illustrates the relationship between the main cutting force and cutting speed for a fiber angle of 45° and a volume fraction of 5%. As shown in the graph, the

Table 6 Error between experimental and simulated values of cutting force

| Simulation scheme | Cutting depth/ μm | Cutting speed/ $\text{m}\cdot\text{min}^{-1}$ | Fiber angle/ $^\circ$ | Fiber material | Cutting force/N(E) | Cutting force/N(S) | Error |
|-------------------|------------------------------|---|-----------------------|----------------|--------------------|--------------------|-------|
| 1 | 30 | 60 | 45 | Al_0 | 8.05 | 7.05 | 12.4% |
| 2 | 40 | 60 | 45 | Al_0 | 8.82 | 7.86 | 10.9% |
| 3 | 50 | 60 | 45 | Al_0 | 10.35 | 9.12 | 11.9% |
| 4 | 60 | 60 | 45 | Al_0 | 11.15 | 9.86 | 11.6% |
| 6 | | | | | | | |

Fig. 4 Surface morphology of CoCrFeNiAl₀ fiber-reinforced aluminum matrix composite under micro-cutting with different cutting depths: **a** 30 μm , **b** 40 μm , **c** 50 μm , **d** 60 μm

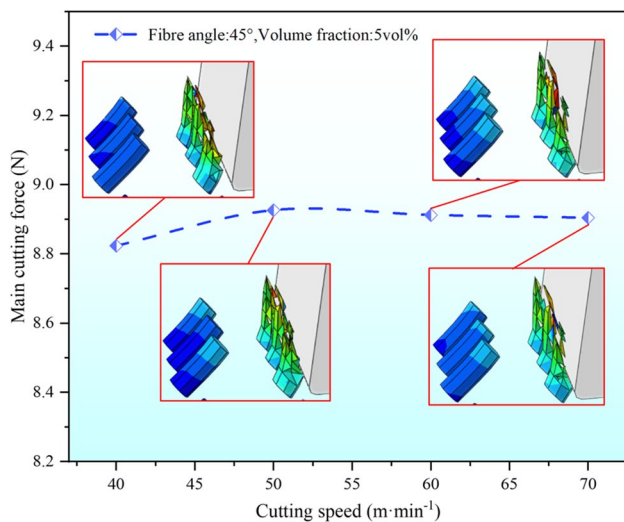
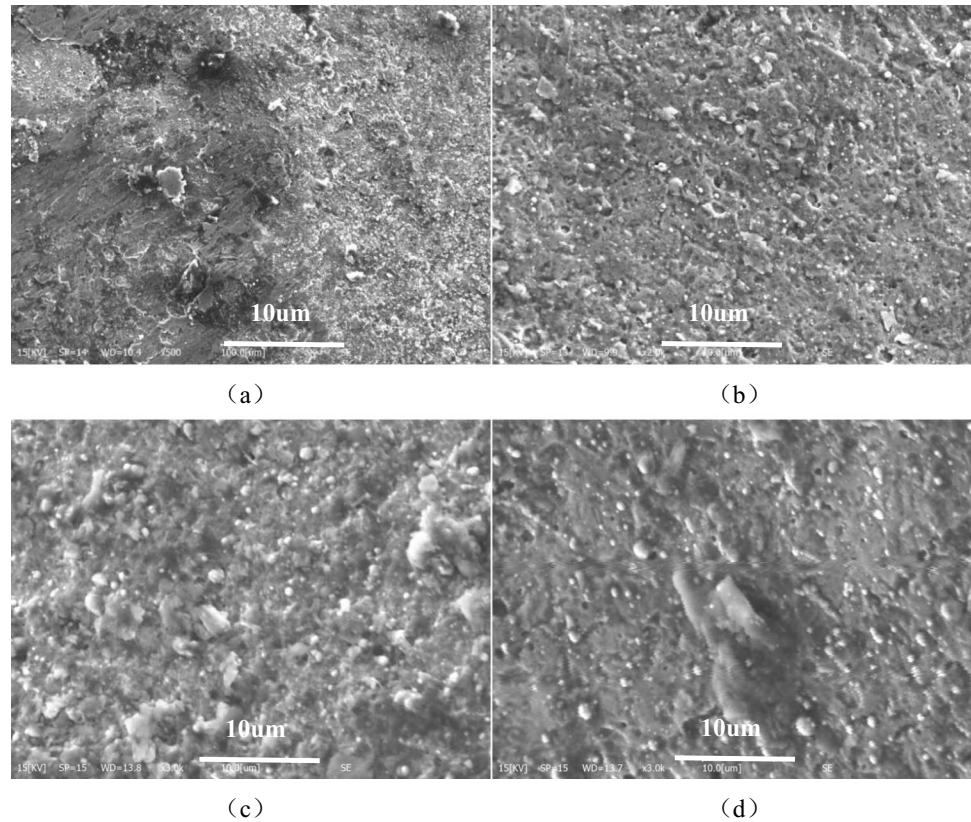


Fig. 5 Relationship between cutting speed and cutting force

cutting force initially increases and then decreases with increasing cutting speed. Analysis suggests that in the cutting process of fiber-reinforced composites, material removal primarily occurs through plastic deformation and fiber fracture. However, within a certain range, the effect of cutting speed on these two cutting mechanisms

is limited. Additionally, due to the good thermal conductivity of fibers and matrix in such composites [31–33], heat can quickly dissipate to areas outside the tool and cutting zone. Therefore, changes in cutting speed have a minor impact on heat, and consequently, a minor effect on cutting force. Thus, there is no significant variation in cutting force. Furthermore, as the cutting speed increases, the temperature in the cutting zone also rises. However, due to the different thermal expansion coefficients between fibers and the matrix in the composite material, the thermal effects lead to increased stress differences between them, resulting in an increase in cutting force. However, when the temperature reaches a certain level, the bonding at the fiber-matrix interface may change [34,35], and the fibers may fracture or detach from the matrix, resulting in a gradual decrease in cutting force. By examining the stress distribution maps under four different cutting speeds, it is evident that an increase in cutting speed from 40 m/min to 50 m/min significantly intensifies stress concentration on the fibers. Similarly, an increase in cutting speed from 50 m/min to 70 m/min leads to a noticeable increase in fiber fracture. This indicates that stress concentration caused by fibers results in an increase in cutting force, while fiber fracture leads to a decrease in cutting force.

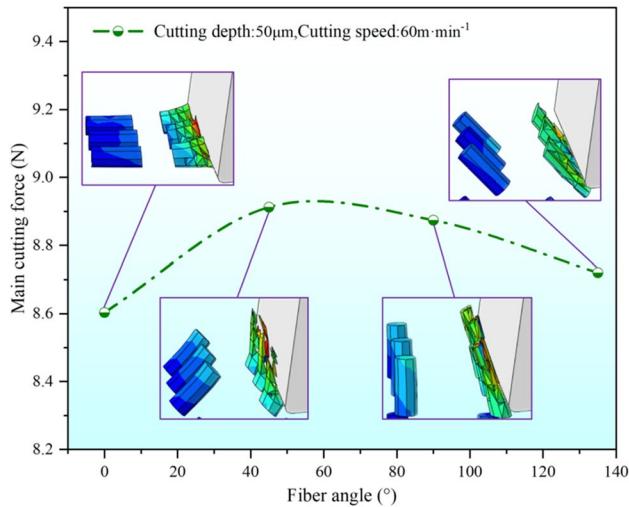


Fig. 6 The relationship between fiber angle and cutting force

3.1.3 Influence of fiber angle on cutting force

Figure 6 illustrates the relationship between the main cutting force and fiber angle for a cutting depth of 50 μm and a cutting speed of 60 m/min. As shown in the graph, the cutting force exhibits a pattern of increasing and then decreasing with the increase in fiber angle. The maximum cutting force of approximately 8.9 N is observed at a fiber angle of 45°. Analysis suggests the following reasons for this behavior: Firstly, when the fiber angle is small, the friction between the fiber and the tool is low. As the fiber angle increases, the friction between the fiber and the tool increases, leading to an increase in cutting force. Secondly, when the fiber angle is small, the fiber is prone to fracture under the action of cutting force, resulting in an increase in cutting force. As the fiber angle further increases, the tensile strength of the fiber increases, making it less prone to fracture, thus reducing the cutting force. At this point, the fiber acts similar to cutting fluid, reducing friction and absorbing some of the cutting heat [36], which further reduces the cutting force. In the case of a fiber angle of 45°, the fiber direction is neither parallel nor perpendicular to the cutting direction of the tool. Therefore, during the cutting process, both shear and tensile forces act on the fiber. When the tool cuts into the material, the shear force on the fiber leads to fiber fracture, while the tensile force on the fiber increases, making it more difficult for the fiber to break. Consequently, under the conditions of a 45° fiber angle, both fiber fracture and fiber tension occur, resulting in the maximum cutting force. On the other hand, when the fiber angle is 0°, the fiber is parallel to the cutting direction, resulting in minimal resistance to cutting force. Additionally, the compression deformation of the fiber also reduces the shear and friction forces between the fiber and the matrix. Consequently, the cutting force is reduced.

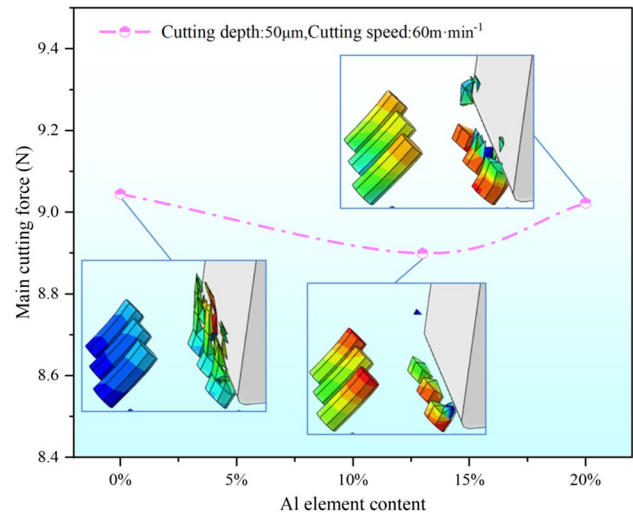


Fig. 7 The relationship between the Al element content in the fiber and the cutting force

Furthermore, the bonding force between the fiber and the matrix increases due to the compression deformation of the fiber, further reducing the cutting force. Therefore, despite experiencing significant compression deformation [37,38], the fiber offers minimal resistance to cutting force when its direction is parallel to the cutting direction. Simultaneously, the shear and friction forces between the fiber and the matrix are reduced, resulting in the smallest cutting force.

Figure 7 shows the relationship between the Al element content in the fiber and the main cutting force for a cutting depth of 50 μm and a cutting speed of 60 m/min. As observed in the graph, the cutting force initially decreases and then increases with increasing Al element content in the fiber. The minimum cutting force is achieved when the Al element content is 13%, approximately 98% of the cutting force for the Al0 fiber–reinforced composite material. Analysis suggests that for CoCrFeNiAl_x short fiber–reinforced composite materials, the variation in Al content affects the material's hardness, stiffness, and plasticity, thereby influencing the magnitude of the cutting force. With an increase in Al content, the formation of hard substances such as Al₂O₃ dispersed in the CoCrFeNiAl_x alloy increases, thereby enhancing the material's hardness and stiffness. This reduces the difficulty of cutting the material, resulting in a decrease in cutting force. Additionally, as the Al content further increases, the grain size in the CoCrFeNiAl_x alloy decreases, and the grain boundaries increase, enhancing the material's ability to undergo plastic deformation [39]. This allows the material to undergo more plastic deformation during the cutting process, thereby increasing the cutting force. When the Al content is 13%, the effects of these two factors offset each other, resulting in the minimum cutting force. Consequently, as the Al content continues to increase, the

effects of increased hardness and stiffness gradually diminish, while the influence of plasticity enhancement becomes more pronounced, leading to an increase in cutting force. By examining the stress distribution maps of different fiber-reinforced cutting models with varying Al content, it can be observed that when the fiber contains no Al element, the fiber exhibits plastic stretching upon contact with the tool. However, when the fiber contains Al, most of the material fractures and disappears due to its higher stiffness under the influence of the damage displacement parameter [40,41]. Among these cases, the fiber with an Al content of 13% exhibits the least remaining fiber portion, resulting in the least obstruction to cutting and thus generating the minimum cutting force.

3.1.4 The influence of fiber content on cutting force

The influence of fiber content on cutting force is shown in Fig. 8 for a cutting depth of 50 μm and a cutting speed of 60 m/min. The graph reveals a positive correlation between cutting force and the volume fraction of fibers in the workpiece. The maximum cutting force is observed when the fiber volume fraction reaches 15 vol%, approximately 1.2 times higher than that of a fiber-free workpiece. Additionally, the largest increase in cutting force, about 16%, occurs when the fiber volume fraction increases from 0 to 5 vol%. Analysis suggests that the addition of fibers enhances the strength and stiffness of the composite material but also increases the difficulty and cutting force during machining. As the fiber volume fraction increases, the number of fibers in the composite material also increases, resulting in enhanced interactions between the fibers and increased stiffness and hardness of the material. This, in turn, increases the difficulty of cutting. Moreover, the increase in fiber volume

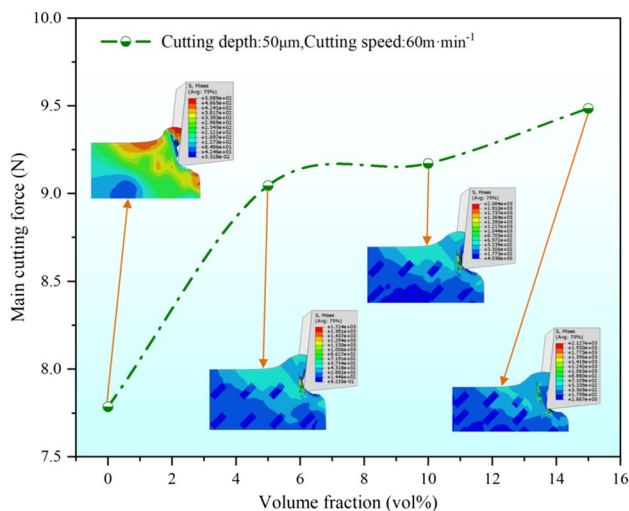


Fig. 8 Relationship between fiber content and cutting force

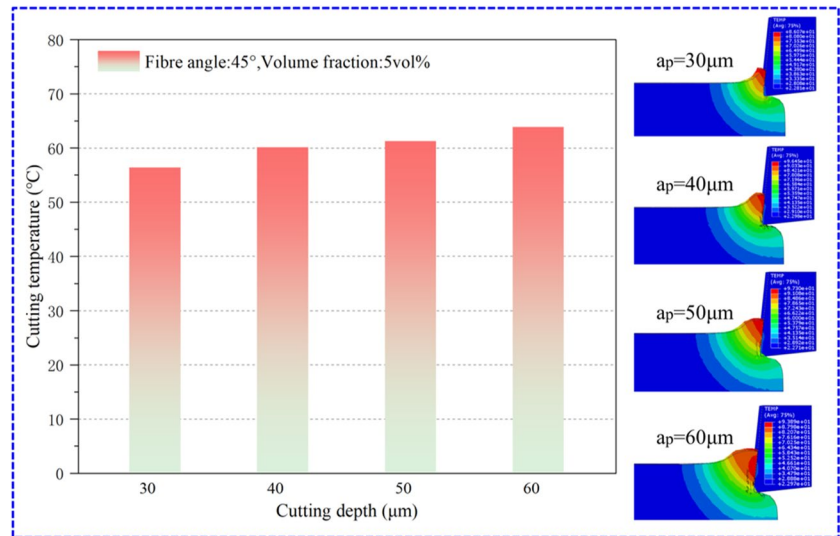
fraction leads to changes in fiber length and spacing, which affect the material's plastic deformation capability [42]. Specifically, an increase in fiber volume fraction reduces the material's plastic deformation capability, resulting in more elastic deformation and cutting shear force during machining. Furthermore, the stress distribution maps of workpieces with different fiber contents demonstrate that the equivalent stress significantly increases with an increase in fiber volume fraction, indicating the importance of stress concentration as a factor affecting cutting force. In summary, an increase in fiber volume fraction increases the difficulty of machining the workpiece, thereby leading to a significant increase in cutting force. Additionally, when the fiber volume fraction is low, the number of fibers in the composite material is limited, resulting in weaker interactions between the fibers and lower stiffness and hardness of the material. Therefore, the addition of fibers from 0 to 5 vol% significantly increases the stiffness and hardness of the material, leading to an increased cutting difficulty and a notable increase in cutting force. Moreover, as the fiber volume fraction continues to increase, the number of fibers in the composite material and their interactions also increase. However, when the fiber volume fraction reaches a certain level, the interactions between fibers become sufficiently strong, and the stiffness and hardness of the material tend to saturate. Consequently, further increases in fiber volume fraction result in diminishing effects on stiffness and hardness, leading to an increase in cutting difficulty and a reduction in the rate of increase in cutting force.

3.2 Cutting temperature analysis

3.2.1 Influence of cutting depth on cutting temperature

Figure 9 shows the relationship between the maximum cutting temperature at the tool tip and the cutting depth, with a fiber angle of 45° and a volume fraction of 5 vol%. As seen from the graph, the cutting temperature gradually increases with the increase in cutting depth. The highest cutting temperature is observed at a cutting depth of 60 μm , reaching approximately 64 °C. Additionally, the temperature contour plot on the right side reveals that the high-temperature region of the chip layer expands with increasing cutting depth. Analysis indicates that in fiber-reinforced composite materials [43], the presence of fibers increases material anisotropy and complexity, making the cutting process more challenging. During cutting, the heat generated by friction between the tool and the workpiece causes temperature rise in the cutting zone. With an increasing cutting depth, the contact area between the tool and the workpiece enlarges, leading to a higher amount of frictional heat and consequently raising the cutting temperature. Furthermore, considering the separation state of the chip layer and the workpiece in the

Fig. 9 Relationship between cutting depth and cutting temperature



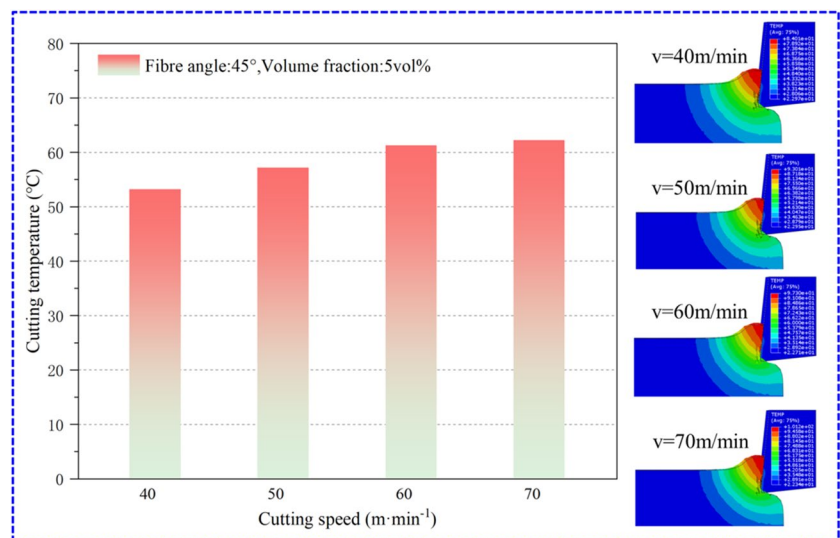
contour plot on the right, the presence of fibers affects the flowability of the chips, resulting in more friction and heat generation during chip flow. Moreover, the fibers in short fiber–reinforced composite materials can experience frictional wear with the chips, further increasing the cutting temperature. Additionally, the fibers may undergo cutting and generate a significant amount of heat, contributing to an elevated cutting temperature. Therefore, as the cutting depth increases, the cutting temperature continues to rise.

3.2.2 Influence of cutting speed on cutting temperature

Figure 10 illustrates the relationship between the maximum cutting temperature extracted at the tool tip and the cutting speed for a fiber angle of 45° and a volume fraction of 5 vol%. As shown in the graph, with an increase in cutting speed, the cutting temperature also rises continuously. The

highest cutting temperature is reached at a cutting speed of 70 m/min, at approximately 62 °C. Additionally, as the cutting speed increases, the increment in cutting temperature gradually decreases, with the maximum increment observed when the cutting speed increases from 40 m/min to 50 m/min, at around 8%. Analysis suggests that in the cutting process of fiber-reinforced composites, an increase in cutting speed leads to higher cutting forces and increased frictional heat, resulting in an elevated cutting temperature. This is because in high-speed cutting, the frictional heat generated in the cutting zone increases with the cutting speed, thereby raising the cutting temperature. However, due to the increased rates of heating and heat dissipation in high-speed cutting, with the heat dissipation rate increasing faster, the increment in cutting temperature diminishes gradually as the cutting speed reaches a certain threshold, eventually reaching an equilibrium state. Furthermore, as the cutting speed

Fig. 10 Relationship between cutting speed and cutting temperature



increases, factors such as plastic deformation and thermal expansion in the material are also enhanced, contributing to the increment in cutting temperature.

3.2.3 Influence of fiber angle on cutting temperature

Figure 11 illustrates the relationship between the highest cutting temperature at the tool tip, with a cutting depth of 50 μm and a cutting speed of 60 m/min, and the fiber angle. As shown in the graph, the cutting temperature exhibits a pattern of initially increasing and then decreasing with the fiber angle. The highest cutting temperature occurs at a fiber angle of 45°, reaching approximately 62 °C, while the lowest cutting temperature occurs at a fiber angle of 135°, measuring around 35 °C, with a decrease of approximately 44%. Analysis suggests that as the fiber angle increases, the component of cutting force in the fiber direction decreases while it increases in the matrix material direction. At a fiber angle of 45°, the cutting force components in both the fiber and matrix material directions are equal, resulting in the maximum cutting force and subsequently the highest cutting temperature. As the fiber angle continues to increase, the component of cutting force in the fiber direction gradually decreases [45], leading to a corresponding decrease in cutting temperature. Moreover, there is a significant difference in thermal conductivity between the fiber material and the matrix material. As the fiber angle increases, the thermal diffusion path in short fiber–reinforced composite materials becomes more complex. At a fiber angle of 45°, heat conduction and diffusion between the fiber and matrix material are least favorable, further contributing to the elevation of cutting temperature. Conversely, at a fiber angle of 135°, the conditions for heat conduction and diffusion are relatively favorable, resulting in a comparatively lower cutting temperature. Additionally, the increase in fiber angle causes

changes in the frictional relationship between the tool and the fibers and matrix material during the cutting process [46]. With smaller fiber angles, the tool is more prone to experience greater friction with the fibers, leading to higher cutting temperatures. As the fiber angle increases, the friction between the fiber and the tool decreases, resulting in a gradual reduction in cutting temperature.

3.2.4 Influence of fiber material on cutting temperature

Figure 12 shows the relationship between the highest cutting temperature at the tool tip and the Al element content in the fibers, with a cutting depth of 50 μm and a cutting speed of 60 m/min. It can be observed from the graph that the cutting temperature exhibits a decreasing-then-increasing trend with increasing Al element content in the fibers. The minimum cutting temperature is achieved when the Al element content is 13%, approximately 60 °C, while the maximum cutting temperature is reached when the Al element content is 20%, approximately 64 °C. Analysis suggests that the increase in Al content raises the melting point of the CoCrFeNiAl_x high-entropy alloy. As a result, higher cutting temperatures are required to achieve the same softening effect with increased Al content. Therefore, at lower Al content, the temperature decreases with increasing Al content. However, the increase in Al content also decreases the thermal conductivity of the CoCrFeNiAl_x high-entropy alloy. Once the Al content reaches a certain level, the decrease in alloy's thermal conductivity offsets the effect of the increased melting point, and even leads to an increase in cutting temperature. When the Al content reaches 13%, the promotion of heat conduction reaches its maximum, resulting in the minimum cutting temperature. However, as the Al content continues to increase to 20%, factors such as interface strength between the fibers and the matrix, fiber length, and distribution start

Fig. 11 Relationship between fiber angle and cutting temperature

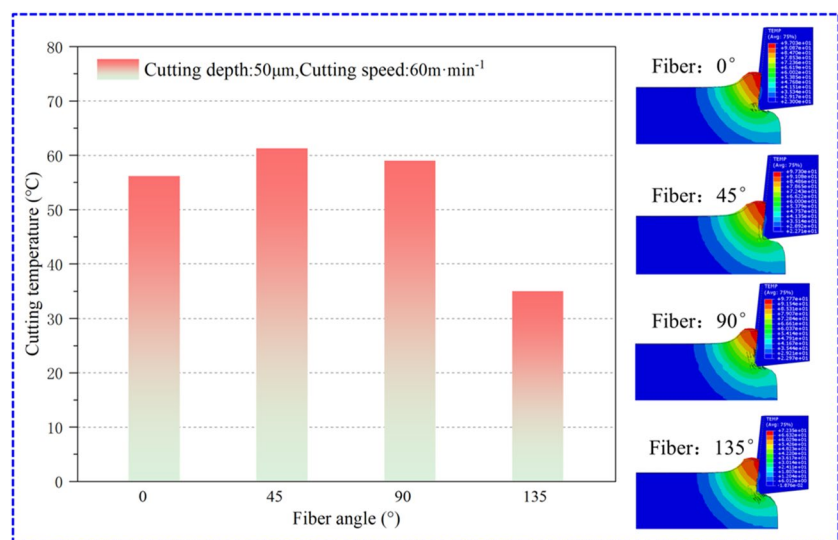
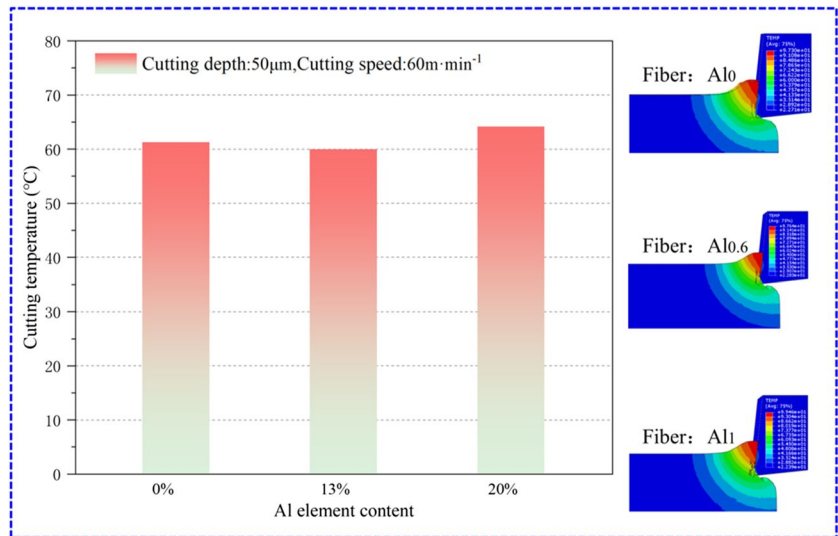


Fig. 12 Relationship between fiber material and cutting temperature



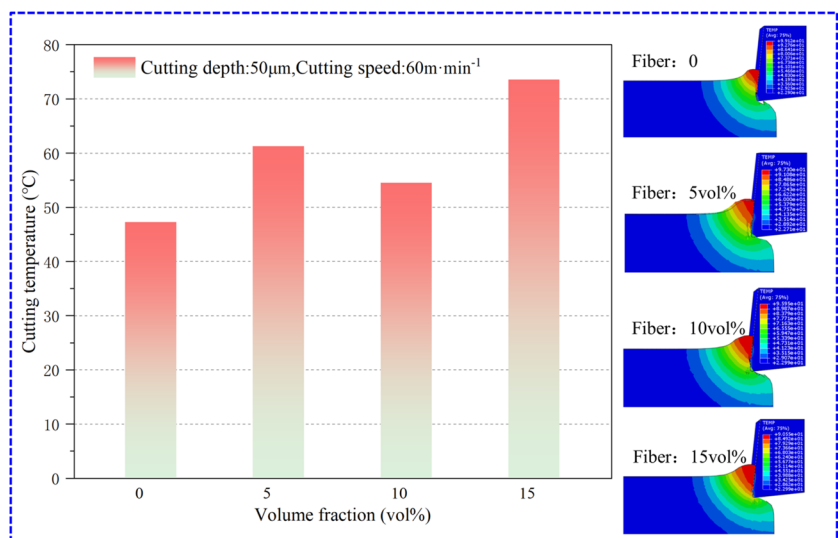
to be affected, resulting in an increase in cutting temperature and reaching the maximum value. Therefore, when the Al content is 20%, the cutting temperature reaches its maximum.

3.2.5 Influence of fiber content on cutting temperature

Figure 13 illustrates the relationship between the highest cutting temperature extracted at the tool tip, with a cutting depth of 50 μm and a cutting speed of 60 m/min, and the fiber content. From the graph, it can be observed that as the volume fraction of fibers increases from 0 to 5%, the cutting temperature significantly rises. During the transition from 5 to 10% fiber volume fraction, the cutting temperature decreases slightly. However, when the fiber volume fraction increases from 10 to 15%, the cutting temperature rises significantly, reaching its

maximum value at approximately 74 °C. Analysis suggests that when the fiber volume fraction increases from 0 to 5%, the addition of fibers enhances the material’s hardness and strength. This leads to increased cutting forces and cutting energy, resulting in an elevated cutting temperature. When the fiber volume fraction increases from 5 to 10%, the frictional heat at the interface between the fibers and the matrix increases. However, due to the high thermal conductivity of fibers, heat conduction and dissipation are enhanced, leading to a slight decrease in cutting temperature. Subsequently, when the fiber volume fraction increases from 10 to 15%, further increasing the fiber volume fraction raises the material’s hardness and strength. This, in turn, causes an increase in cutting forces and cutting energy, while the enhancement in heat conduction is relatively limited, resulting in a subsequent rise in cutting temperature.

Fig. 13 Relationship between Fiber Content and Cutting Temperature



3.3 Analysis of chip morphology

3.3.1 Influence of cutting depth on chip morphology

Figure 14 shows the chip morphology at different cutting depths. It can be observed that with increasing cutting depth, the thickness and integrity of the chips significantly improve. When the cutting depth is $30\ \mu\text{m}$, the chips appear fragmented. When the cutting depth is $60\ \mu\text{m}$, the chips exhibit larger thickness and fewer fractured segments. Additionally, the peak value of Mises stress and its concentration range gradually increase with the increase in cutting depth. Analysis suggests that during the cutting process, as the cutting depth increases, the cutting forces also increase, leading to changes in chip morphology. In the initial stage with a small cutting depth, the cutting forces are low, and only a small portion of fibers fracture, resulting in fragmented chips. However, as the cutting depth increases, the cutting forces gradually increase, and the number of fiber fractures also increases. Simultaneously, the fractured fibers are distributed more evenly within the chips, thereby improving chip integrity. Moreover, at lower cutting depths, the chip formation process is more susceptible to fiber disturbance and cutting [47], leading to chip fragmentation. On the other hand, larger cutting depths correspond to longer chip sliding distances, generating higher stress and strain within the chip. When the stress exceeds the material's strength, chip fracture occurs. However, the longer sliding distance also provides more time and space for the chip to relieve and disperse

these stresses, promoting the formation of intact chips. Increasing cutting depth causes the generation of cutting forces and stresses to move deeper into the cutting region, resulting in an increased concentration range of stress. Furthermore, as the cutting depth increases, the number of fiber fractures during the cutting process also gradually increases, leading to stress concentration around the fractured fibers and an increase in peak stress values.

3.3.2 Influence of fiber angle on chip morphology

Figure 15 represents the chip morphology at different fiber angles. It can be observed that when the fiber angle is 45° or 90° , the chip integrity is poor, with a higher number of fragmented chips and irregular shapes. On the other hand, when the fiber angle is 0° or 135° , the chip integrity is better, with fewer fragmented chips and more regular shapes. Additionally, the stress concentration region is larger for fibers at 0° or 90° compared to fibers at 45° or 135° . Analysis suggests that in short fiber-reinforced composites, the fiber angle influences the mechanical properties of the material and the cutting behavior during machining. When the fiber angle is 45° or 90° , the cutting tool cuts along the direction of the fibers, making the fibers more prone to separation and fracture during the cutting process. However, when the fiber angle is 0° or 135° , the relative motion between the cutting tool and the fibers is nearly perpendicular, resulting in a lower probability of fiber separation and fracture during cutting. At fiber angles of 45° or 90° , the chip formation mechanism

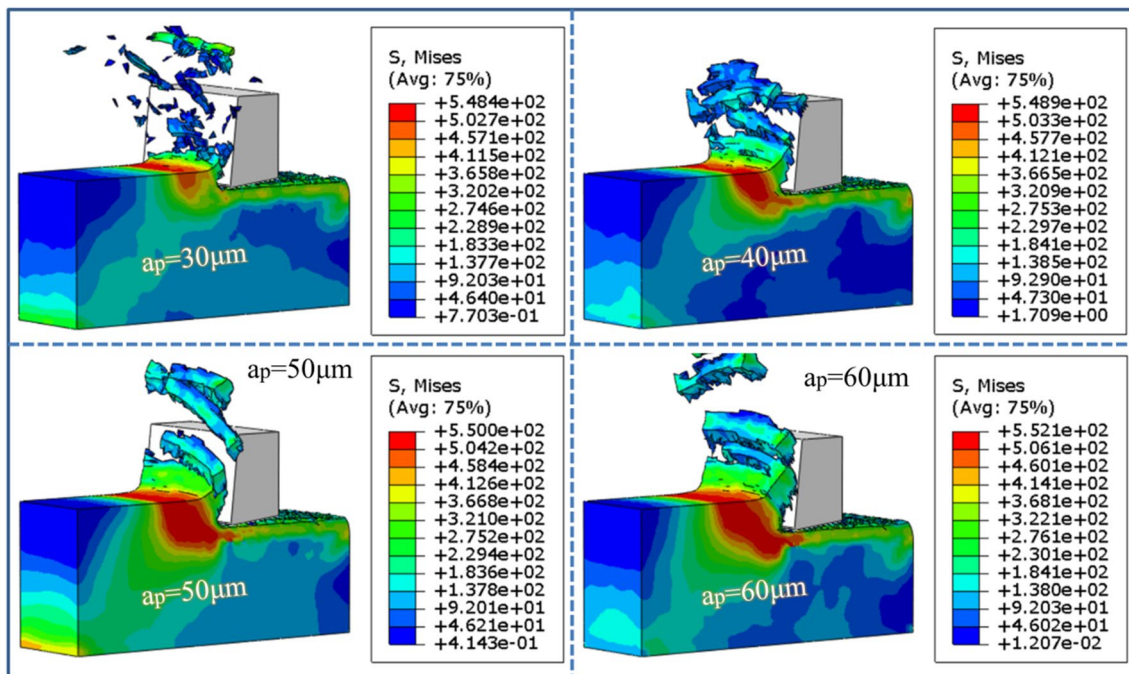


Fig. 14 The chip morphology at different cutting depths

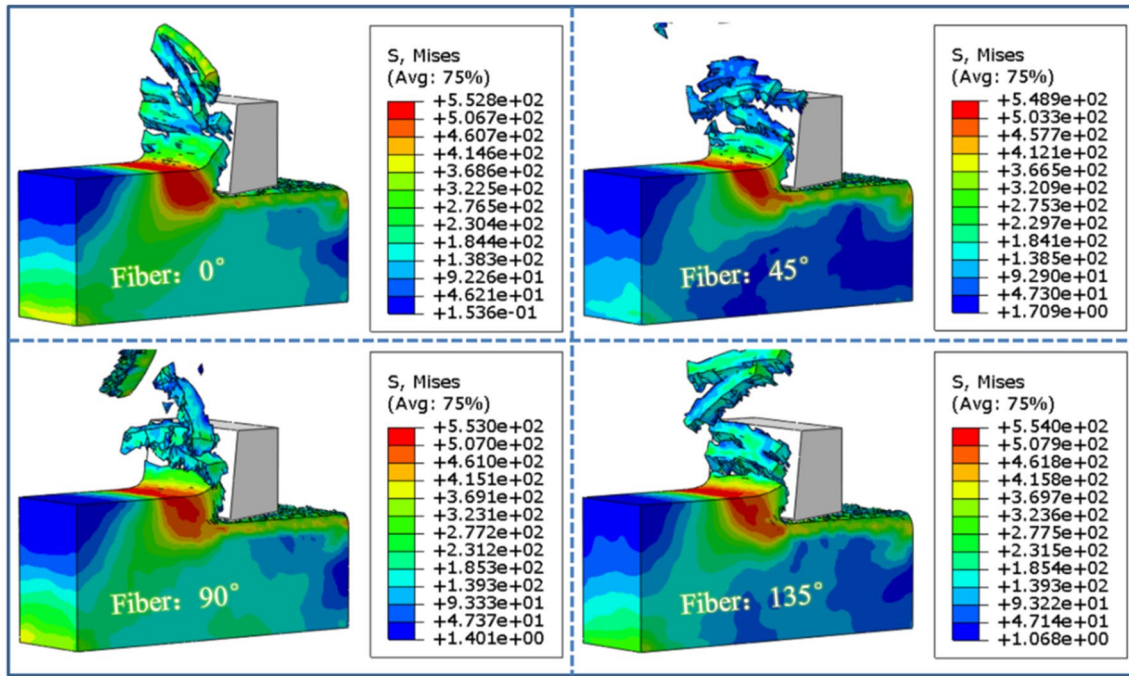


Fig. 15 Chip morphology at different fiber angles

primarily involves fiber bending and stretching [48]. In such cases, the chips produced are prone to fragmentation and deformation. Conversely, at fiber angles of 0° or 135°, the chip formation mechanism mainly involves shearing of the matrix material and cutting of the fibers. This results in better chip integrity, with fewer fragmented chips and more regular shapes. At fiber angles of 0° or 90°, the stress during cutting primarily concentrates at the interface between the fibers and the matrix material. Due to the significant mechanical property difference between the fibers and the matrix material, the stress concentration region is larger. In contrast, at fiber angles of 45° or 135°, the angle between the cutting direction and the fiber direction is smaller, resulting in a more uniform stress distribution between the fibers and the matrix material, and thus a smaller stress concentration region. At fiber angles of 0° or 90°, the efficiency of stress transfer between the fibers and the matrix material is lower,

leading to a larger stress concentration at the fiber-matrix interface. Conversely, at fiber angles of 45° or 135°, the efficiency of stress transfer between the fibers and the matrix material is higher, which helps reduce the extent of stress concentration regions.

3.3.3 Influence of fiber material on chip morphology

Figure 16 shows the chip morphology at different fiber contents. It can be observed that as the Al content in the fiber material increases, the number of fragmented chips decreases and their shape becomes more regular. The peak value of Mises stress and its concentrated range also increase significantly. When the fiber material is CoCrFeNiAl_x, the strength and stiffness of the composite material gradually increase with the increasing Al content in the fibers. This is due to the high strength and stiffness of Al, which effectively

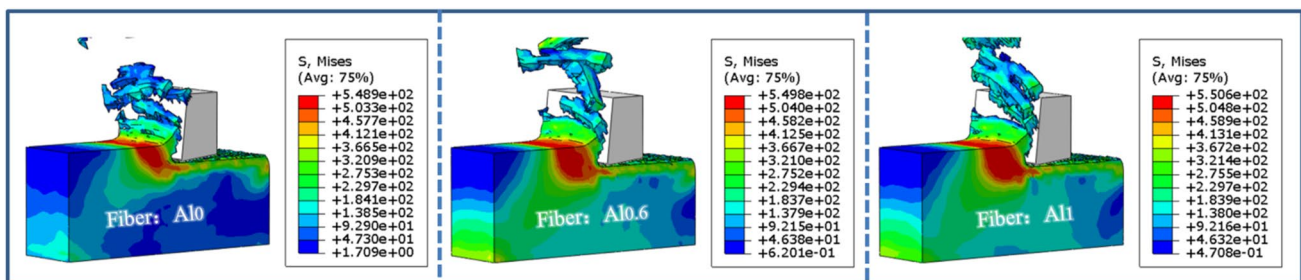


Fig. 16 Chip morphology at different fiber materials

resists further penetration of the cutting edge and increases the tensile and shear strength of the material, thereby reducing shear deformation and fracture. This leads to a gradual reduction in the number of fragmented chips and their shape becoming more regular. Furthermore, when the Al content is high, the high-entropy effect of CoCrFeNiAl_x alloy is further enhanced, improving the material's uniformity and interface bonding strength. This also helps reduce the number of fragmented chips and promote a regular chip morphology. Moreover, with the increase in Al content, the stress distribution in the composite material changes [49]. Due to the high strength and stiffness of Al, the required stress for its fracture also increases, resulting in a significant increase in stress peak value and concentration range in the material. Additionally, CoCrFeNiAl_x high-entropy alloy has a uniform microstructure and good compositional uniformity, and the interface bonding strength between the fiber and matrix materials is also high. These advantages make CoCrFeNiAl_x composite materials exhibit good resistance to cutting and regular chip formation during machining, contributing to improved surface quality and processing efficiency.

3.3.4 Influence of fiber content on chip morphology

Figure 17 shows the chip morphology at different fiber contents. From the figure, it can be observed that the shape of the chips becomes more complex when the fiber content is 0. However, as the fiber content gradually increases, the shape of the chips becomes more regular. When the fiber

volume fraction reaches 15 vol%, the chip layer exhibits regularly fractured block-like chips of similar volume. Additionally, with the increase in fiber content, the peak value of Mises stress and its concentration range also gradually increase. In short fiber-reinforced composites, the presence of fibers can effectively enhance the strength and stiffness of the material, but it also affects its machining performance [50]. During the machining process, the cutting tool applies shear stress to the material, causing shear deformation and fracture. The shape and size of the fractured chips have a significant impact on the surface quality and machining efficiency of the material. When the fiber content is 0, there are no reinforcing phases in the material, and the fracture behavior is primarily controlled by the matrix material. Due to the relatively uniform structure of the matrix material, the shape of the fractured chips is complex and irregular. However, as the fiber content gradually increases, the presence of the reinforcing phase alters the fracture behavior of the material. When the volume fraction of fibers reaches a certain level, the interaction between fibers restricts the expansion of the chip layer, leading to localized chip fracture and the formation of similarly sized block-like chips. When the fiber content reaches a certain level, the shape of the chips gradually becomes more regular [51], exhibiting block-like characteristics. Furthermore, with the increase in fiber content, the strength and stiffness of the material increase, and the concentration range of stress also expands. During the machining process, the fibers in the material impede

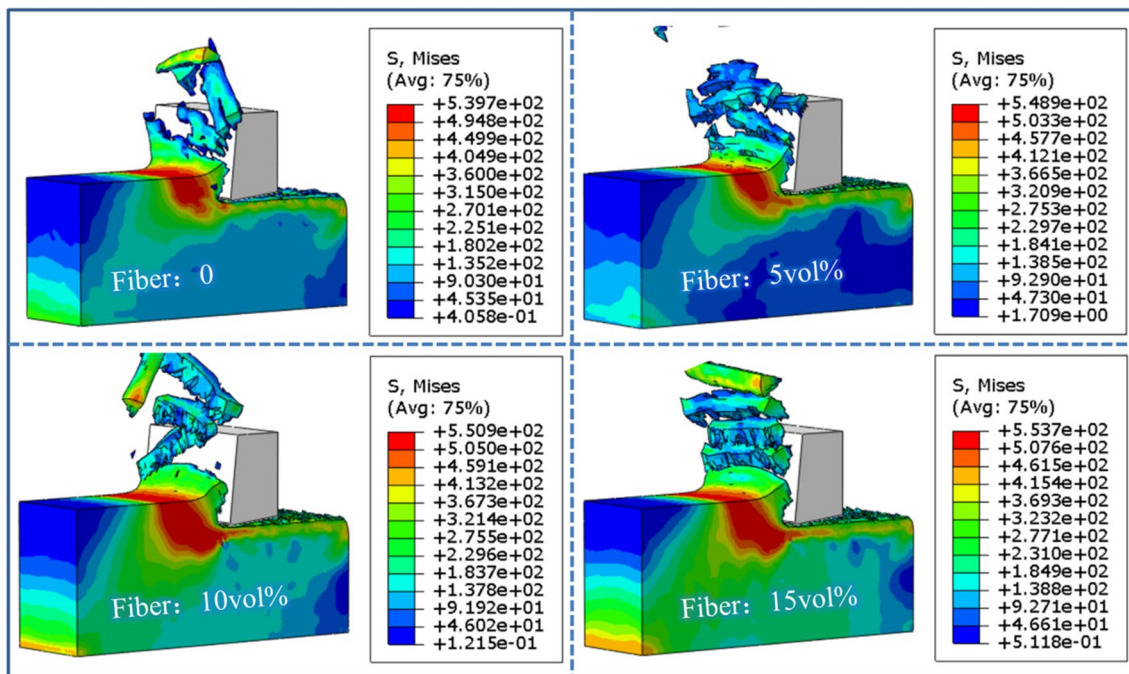


Fig. 17 The chip morphology at different fiber contents

further penetration of the cutting tool, causing stress to concentrate in the matrix material surrounding the fibers. This leads to an increase in the peak value and concentration range of stress.

3.4 Residual stress analysis

3.4.1 Influence of cutting depth on residual stress

Figure 18 shows the residual stress curves at different cutting depths. It can be observed from the graph that the peak residual compressive stress is negatively correlated with the cutting depth, and the peak position moves away from the machined surface as the cutting depth increases. As the cutting depth increases, the depth of tool penetration also increases, resulting in the cutting or shearing of fibers during the cutting process, thereby reducing the strength-enhancing effect of the fibers on the material. This leads to a decrease in the overall strength of the material, resulting in a gradual reduction in the peak value of residual compressive stress. Additionally, during the cutting process, the roughness and morphology of the machined surface change accordingly, altering the stress distribution in the material and thus affecting the residual compressive stress. With the increase in cutting depth, the changes in surface condition become more significant, leading to the peak of residual compressive stress moving away from the machined surface. Furthermore, variations in processing temperature also influence the stress distribution in the material and, consequently, the residual compressive stress. With the increase in cutting depth, the temperature changes during machining become

more pronounced, resulting in a gradual reduction in the peak value of residual compressive stress.

3.4.2 The influence of cutting speed on residual stress

Figure 19 shows the residual stress curves at different cutting speeds. It can be observed from the graph that the peak residual compressive stress is inversely correlated with cutting speed, and the position of the peak also moves away from the machined surface as the cutting speed increases. Analysis suggests that an increase in cutting speed leads to a higher material temperature, resulting in enhanced plastic deformation capacity. Consequently, the material is more prone to undergo plastic deformation during the cutting process, reducing the accumulation of residual compressive stress. Additionally, due to the shorter length of short fibers, their interaction forces are weaker, making them susceptible to fracture and delamination during cutting. As the cutting speed increases, the probability of fiber fracture and delamination also increases, leading to a decrease in residual compressive stress. Moreover, the elevated temperature in the cutting zone caused by higher cutting speeds results in a larger coefficient of thermal expansion for the material, causing the peak residual compressive stress to shift inward. Furthermore, factors such as changes in fiber orientation and fiber fracture can influence the material’s strength and hardness, thereby affecting the position of the peak residual compressive stress.

3.4.3 Effect of fiber angle on residual stress

Figure 20 shows the residual stress curves under different fiber angles. It can be observed from the graph that the peak value of residual compressive stress is positively correlated

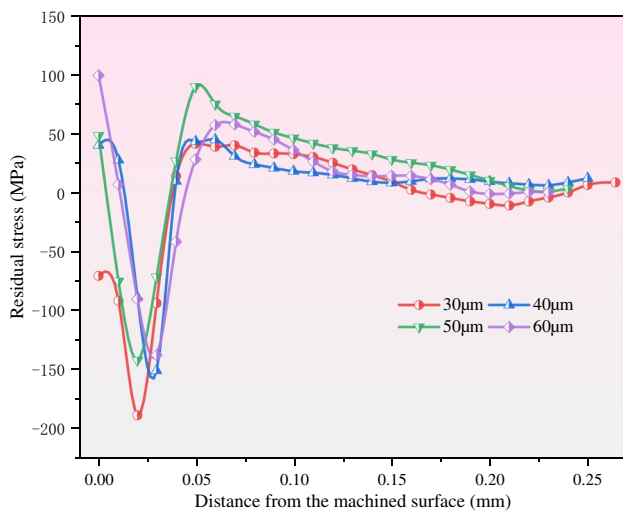


Fig. 18 The residual stress curves at different cutting depths

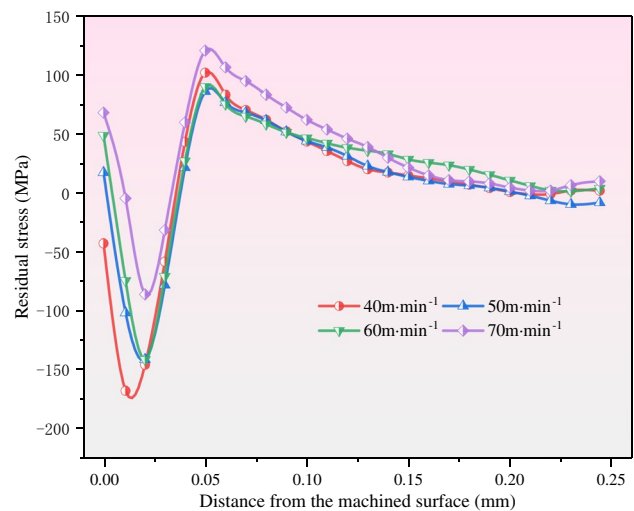


Fig. 19 Residual stress curves under different cutting speeds

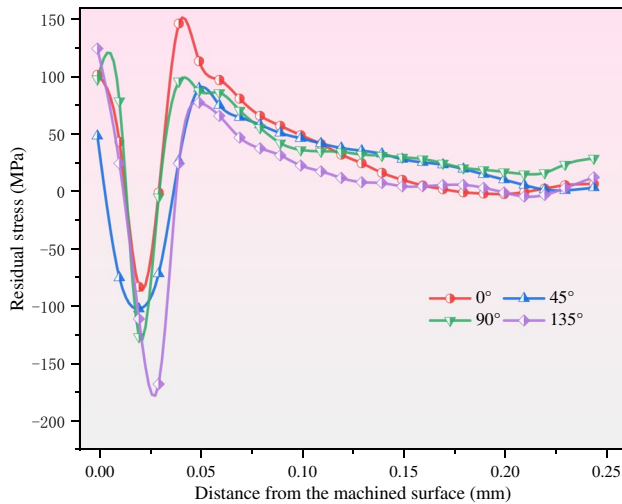


Fig. 20 Residual stress curves under different fiber angles

with the fiber angle, and only when the fiber angle is 135° , the peak value position significantly moves away from the machining surface. Analysis suggests that the variation in fiber angle affects the mechanical properties of the material. When the fiber angle has a smaller deviation from the cutting direction, the resistance to fiber cutting is lower, resulting in longer residual fiber lengths after fracture and relatively smaller residual compressive stress generated during the cutting process. On the other hand, when the fiber angle deviates more significantly from the cutting direction, the resistance to fiber cutting increases, leading to shorter residual fiber lengths after fracture and relatively higher residual compressive stress formed during cutting. Additionally, when the fiber angle is 135° , the shorter residual fiber length after fracture contributes to the deeper peak of residual compressive stress below the surface. In contrast, for other fiber angles, longer residual fiber lengths result in peak residual compressive stress occurring at shallower depths, closer to the surface.

3.4.4 Influence of fiber material on residual stress

Figure 21 shows the residual stress curves under different fiber materials. It can be observed that the peak value of residual compressive stress is negatively correlated with the Al content in the fibers, while the peak position remains relatively unchanged. Analysis suggests that when the Al content in the fibers increases, the hardness and strength of the alloy typically decrease. This is because Al reduces the deformation hardening capacity and interfacial strength of the alloy. Therefore, a higher Al content in the fibers weakens the resistance of the fibers, resulting in increased cutting force and peak value of residual compressive stress. Additionally, when the material is subjected to thermal

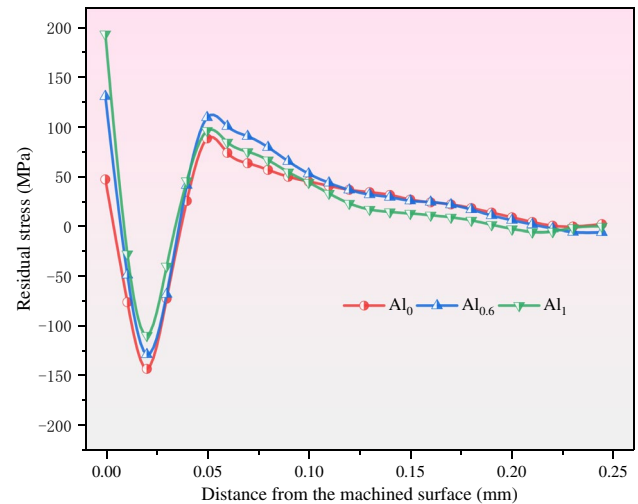


Fig. 21 Residual stress curves under different fiber materials

influence during the cutting process, a higher Al content in the fibers leads to an increase in the material's thermal expansion coefficient. This, in turn, results in greater thermal expansion deformation of the material, thereby affecting the distribution of residual stress.

3.4.5 The influence of fiber content on residual stress

Figure 22 depicts the residual stress curves for different fiber contents. It can be observed that the peak residual compressive stress is positively correlated with the fiber content, and the peak position is significantly distant from the machined surface only when the fiber volume fraction is 15 vol%. Analysis suggests that as the fiber content increases, the resistance provided by the fibers also

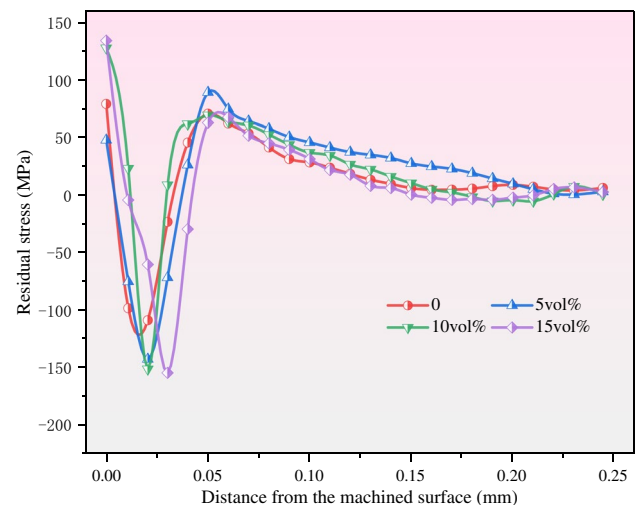


Fig. 22 Residual stress curves at different fiber contents

increases. This enhanced resistance effectively counteracts the cutting forces during the machining process, leading to higher cutting forces and peak residual compressive stress. Moreover, the fiber volume fraction also affects the distribution of residual stress. At lower fiber volume fractions, the resistance provided by the fibers is relatively weaker, resulting in smaller cutting forces and peak residual stress values that are closer to the surface. As the fiber volume fraction increases, the resistance provided by the fibers strengthens, leading to higher cutting forces and peak residual stress values. Notably, at a fiber volume fraction of 15 vol%, the resistance provided by the fibers is maximized, causing the peak residual stress to be significantly distant from the machined surface. This indicates that different cutting parameters and tool designs should be employed to optimize the machining performance based on the specific fiber content and volume fraction.

4 Conclusion

This study employed the ABAQUS finite element software to simulate the micro-cutting process of CoCrFeNiAl_x short fiber-reinforced 7A09 aluminum-based composite material. The effects of different cutting parameters on the fiber angle, volume fraction, and Al element content of the short fibers on cutting force, cutting temperature, chip morphology, and residual stress were investigated. The following conclusions can be drawn:

- (1) Cutting depth is positively correlated with cutting force, and the cutting force at 60 μm is approximately 1.5 times that at 30 μm. With the increase in cutting speed and fiber angle, the cutting force initially increases and then decreases. However, with an increase in Al element content in the fibers, the cutting force exhibits a decreasing-then-increasing trend, reaching its minimum when the Al element content is 13%. The cutting force increases continuously with the increase in fiber volume fraction in the workpiece and reaches its maximum when the volume fraction is 15 vol%, which is approximately 1.2 times that of the workpiece without fibers.
- (2) Cutting temperature gradually increases with the increase in cutting depth and cutting speed. Among them, the cutting temperature reaches its peak when the cutting depth is 60 μm and the cutting speed is 70 m/min, reaching approximately 63 °C. With an increase in fiber angle, the cutting temperature initially rises and then decreases. The cutting temperature is highest when the fiber angle is 45°, reaching approximately 62 °C, while it is lowest when the fiber angle is 135°, reaching approximately 35 °C, representing a reduction of approximately 44%. The cutting temperature shows a decreasing-then-increasing trend with an increase in Al element content in the fibers. The cutting temperature is at its minimum when the Al element content is 13%, approximately 60 °C, and it is at its maximum when the Al element content is 20%, approximately 64 °C. The cutting temperature exhibits complex changes of increase, decrease, and subsequent increase with an increase in fiber volume fraction.
- (3) The thickness and integrity of chips significantly improve with the increase in cutting depth. When the fiber angle is 45° or 90°, the chips are more fragmented and irregular, while the chip integrity improves when the fiber angle is 0° or 135°. The integrity of chips noticeably improves with an increase in Al content in the fibers. Complex chip shapes are obtained when the fiber content is 0, but as the fiber content gradually increases, the chip shape becomes more regular. When the fiber volume fraction reaches 15 vol%, similar-sized block chips are generated. Additionally, the peak of Mises stress and the range of stress concentration increase with the increase in cutting depth, Al content in the fibers, and fiber volume fraction in the workpiece.
- (4) The peak value of residual stress is negatively correlated with cutting depth, cutting speed, and Al element content in the fibers, and the peak position moves away from the machined surface with an increase in the first two factors. The peak value of residual stress is positively correlated with fiber angle and fiber content in the workpiece. When the fiber angle is 135° or the fiber volume fraction is 15 vol%, the peak position of residual stress is noticeably far from the machined surface.

Author contribution The design of the overall scheme was completed by ZP. The design of the simulation scheme was completed by WS and LZ. Data extraction was completed by GY and YX. Language modification was completed by ZS.

Funding The work was supported by the National Natural Science Foundation of China(51705270), the National Natural Science Foundation of China (No.51575289), the Natural Science Foundation of Guangdong Province (No.2023A1515030171), the Science and Technology Project of Zhanjiang City, Guangdong Province(No.2022A01004), the Natural Science Foundation of Shandong Province (No.ZR2016EEP03), the Applied Basic Research Program of Qingdao city(No.19-6-2-69-cg), and the Shandong Qingchuang Science and Technology Project (No.2019KJB022).

Data availability The authors confirm that all data are true and reliable.

Code availability The software is reliable.

Declarations

Ethics approval There are no ethical issues with manuscripts.

Consent to participate All the authors of the manuscript agreed to participate.

Consent for publication All the authors of the manuscript agreed to publish this paper in the International Journal of Advanced Manufacturing Technology.

Conflict of Interest The authors declare no competing interests.

References

- Srinivasan V, Kunjiappan S, Palanisamy P (2021) A brief review of carbon nanotube reinforced metal matrix composites for aerospace and defense applications [J]. *Int Nano Lett* 11(4):321–345
- Lei C, Man Z, Zhutang W (2020) Application and production overview of aluminum-based composites in civil aircraft in China [J]. *Light Alloy Fabr Technol* 48(02):1–7
- Zhang LC, Zhang HJ, Wang XM (2001) A force prediction model for cutting unidirectional fibre-reinforced plastics. *Mach Sci Technol* 5(3):293–305
- Zhang LC (2008) Cutting composites: a discussion on mechanics modelling [J]. *J Mater Process Tech* 209(9):4548–4552
- Wang DH, Ramulu M, Arola D (1995) Orthogonal cutting mechanisms of graphite/epoxy composite. Part I: unidirectional laminate [J]. *Int J Mach Tools Manuf* 35(12):1623–1638
- Wang XM, Zhang LC (2003) An experimental investigation into the orthogonal cutting of unidirectional fibre reinforced plastics [J]. *Int J Mach Tools Manuf* 43(10):1015–1022
- Marques AT, Durão LM, Magalhães AG et al (2009) Delamination analysis of carbon fibre reinforced laminates: evaluation of a special step drill [J]. *Compos Sci Technol* 69(14):2376–2382
- Shyha IS, Aspinwall DK, Soo SL et al (2009) Drill geometry and operating effects when cutting small diameter holes in CFRP [J]. *Int J Mach Tools Manuf* 49(12–13):1008–1014
- Rajasekaran T, Palanikumar K, Vinayagam BK (2011) Application of fuzzy logic for modeling surface roughness in turning CFRP composites using CBN tool [J]. *Prod Eng Res Dev* 5:191–199
- Palanikumar K (2008) Application of Taguchi and response surface methodologies for surface roughness in machining glass fiber reinforced plastics by PCD tooling [J]. *Int J Adv Manuf Technol* 36(1–2):19–27
- Cheng H, Gao J, Kafka OL et al (2017) A micro-scale cutting model for UD CFRP composites with thermo-mechanical coupling [J]. *Compos Sci Technol* 153:18–31
- Chen Y, Zhang X, Dunand DC et al (2009) Shape memory and superelasticity in polycrystalline Cu–Al–Ni microwires [J]. *Appl Phys Lett* 95(17):171906
- Shengguo Ma, Zhihua W (2021) Dynamic mechanical properties and constitutive relations of CoCrFeNiAl_x High-Entropy Alloys [J]. *Explosion Shock Waves* 41(11):4–14
- Wu X et al (2021) Investigation on the machining performance of carbon fiber reinforced aluminum matrix composites. *Compos Part B: Eng* 226:109109
- Zhang L et al (2021) Influence of fiber orientation on the machinability of carbon fiber-reinforced aluminum matrix composites. *Compos Part B: Eng* 208:108715
- Yang Y et al (2021) Machining behavior and surface integrity of carbon fiber reinforced aluminum matrix composites. *Materials* 14(6):1374
- Li Y et al (2020) Experimental and numerical investigation on machining carbon fiber reinforced aluminum matrix composites. *J Mater Process Technol* 277:116429
- Li Z et al (2020) Machinability study on carbon fiber reinforced aluminum matrix composites based on cutting force and surface roughness. *J Compos Mater* 54(28):4019–4032
- Liu X et al (2004) Machining characteristics of SiC particle reinforced aluminum matrix composites. *J Mater Process Technol* 148(3):338–343
- Sornsuwit N et al (2006) An experimental investigation into the machining characteristics of aluminum matrix composites reinforced with SiC particles. *J Mater Process Technol* 178(1–3):141–148
- Serkan K, Gokhan A, Izzet K (2023) An experimental study on the cutting depth produced by abrasive waterjet: how do abrasive and rock properties affect the cutting process? [J]. *Int J Adv Manuf Technol*. <https://doi.org/10.1007/s00170-023-11053-5>
- Aydin G, Karakurt I, Amiri MR, Kaya S (2022) Improvement of rock cutting performance through two-pass abrasive waterjet cutting. *Sustainability* 14(19):12704. <https://doi.org/10.3390/su141912704>
- Kukliński M, Bartkowska A, Przystacki D (2018) Investigation of laser heat treated monel 400. *MATEC Web Conf* 219(5):02005
- Przystacki D, Chwalczuk T (2017) The analysis of surface topography during turning of Waspaloy with the application of response surface method (eds). *Proc 2017 2nd Int Conf Des Mech Mater Eng* 11(4):88–93
- Zhang P, Liu ZH, Liu JL, Yu J, Mai QQ, Yue XJ (2023) Effect of aging plus cryogenic treatment on the machinability of 7075 aluminum alloy. *Vacuum* 208:111692. <https://doi.org/10.1016/j.vacuum.2022.111692>
- Zhang P, Liu ZH, Yue XJ, Wang PH, Zhai YC (2022) Water jet impact damage mechanism and dynamic penetration energy absorption of 2A12 aluminum alloy. *Vacuum* 206:111532. <https://doi.org/10.1016/j.vacuum.2022.111532>
- Niu Z, Jiao F, Cheng K (2018) An innovative investigation on chip formation mechanisms in micro-milling using natural diamond and tungsten carbide tools. *J Manuf Process* 31(1):382–394
- Cheng K, Huo D (2013) *Micro cutting: fundamentals and applications*. John Wiley & Sons, Chichester
- Wu W et al (2007) Machining of Al/SiCp metal matrix composites: a study on the tool wear mechanisms. *J Mater Process Technol* 191(1–3):351–354
- Yigit R et al (2008) Machining of particle reinforced metal matrix composites: an experimental study. *J Mater Process Technol* 199(1–3):429–436
- Huang C et al (2019) Experimental investigation of cutting forces and surface roughness in milling SiCp/Al composites. *Int J Adv Manuf Technol* 104(1–4):871–879
- Guo H et al (2019) Experimental study on the machinability of SiCp/Al composites in turning. *Materials* 12(14):2204
- Zhang P, Liu JL, Gao YR, Liu ZH, Mai QQ (2023) Effect of heat treatment process on the micro machinability of 7075 aluminum alloy. *Vacuum* 207:111574. <https://doi.org/10.1016/j.vacuum.2022.111574>
- Zhang P, Wang S, Lin Z, Yue X, Gao Y, Zhang S, Yang H (2023) Investigation on the mechanism of micro-milling CoCrFeNiAl_x high entropy alloys with end milling cutters. *Vacuum*. <https://doi.org/10.1016/j.vacuum.2023.111939>
- Zhang P, Lin Z, Liu Z, Liu J, Mai Q, Yue X (2023) Effect of cutting parameters on the microstructure evolution and damage mechanism of 7075-T6 aluminum alloy in micro cutting. *Int J Damage Mech* 32(7):9194–939. <https://doi.org/10.1177/10567895231171408>

36. Bhattacharyya B et al (2019) An experimental investigation on the machinability of aluminum metal matrix composites reinforced with SiC and Al₂O₃ particulates. *J Compos Mater* 53(23):3259–3272
37. Arsecularatne JA et al (2009) Machining of metal matrix composites. *CIRP Ann* 58(2):592–609
38. Khairyanto A et al (2010) Tool wear characteristics in the milling of SiC particle reinforced aluminum matrix composites. *J Mater Process Technol* 210(1):56–63
39. Patil RP et al (2011) Machinability study of aluminium matrix composites—a review. *Int J Manuf Res* 6(4):360–387
40. Rajmohan T et al (2012) Experimental investigation on machining characteristics of Al/SiCp metal matrix composites. *Mater Manuf Processes* 27(8):839–844
41. Zhao J et al (2013) Cutting force modeling in drilling of aluminum matrix composites reinforced by SiC particles. *Int J Adv Manuf Technol* 66(5–8):839–846
42. Sharma S et al (2014) An experimental investigation on the machinability aspects of Al6061-SiCp metal matrix composites using WEDM. *J Mater Process Technol* 214(4):868–879
43. Suresh R et al (2015) Experimental investigation on machinability of Al/SiC metal matrix composites using wire electrical discharge machining. *Procedia Eng* 132:654–660
44. Wang ZJ et al (2016) Experimental study on machining characteristics and machinability of particle reinforced metal matrix composites. *Int J Adv Manuf Technol* 87(1–4):423–431
45. Lim JK et al (2017) Experimental investigation on machinability of Al/SiC metal matrix composites with PCD and CVD diamond-coated tools. *J Manuf Process* 25:209–217
46. Ahmed MMZ et al (2018) Effect of cutting parameters on surface roughness and cutting forces in high-speed milling of Al/SiCp metal matrix composites. *Mater Manuf Processes* 33(12):1369–1378
47. Raza MA et al (2018) Experimental investigation of machinability characteristics of aluminum based composites reinforced with carbon and ceramic particles. *J Compos Mater* 52(4):517–526
48. Ramesh M et al (2020) Machinability investigation of carbon fiber reinforced aluminum matrix composites using coated carbide tool. *J Market Res* 9(4):8976–8987
49. Qiu X, Li P, Li C, Niu Q, Chen A, Ouyang P, Ko TJ (2018) Study on chisel edge drilling behavior and step drill structure on delamination in drilling CFRP. *Compos Struct* 203:404–413
50. Zhang P, Gao Y, Zhang S et al (2023) The Mechanism of the Effect of Dual-Sided Waterjet Peening on the Surface Integrity and Fatigue Performance of 12 mm Thick Inconel 718 [J]. *Int J Fatigue* 178:1–19
51. Chen X et al (2019) Experimental study on cutting forces and surface roughness in machining of SiCp/Al composites. *Int J Adv Manuf Technol* 104(1–4):1095–1104

Publisher's Note Springer Nature remains neutral with regard to jurisdictional claims in published maps and institutional affiliations.

Springer Nature or its licensor (e.g. a society or other partner) holds exclusive rights to this article under a publishing agreement with the author(s) or other rightsholder(s); author self-archiving of the accepted manuscript version of this article is solely governed by the terms of such publishing agreement and applicable law.